Thermal radiative fluxes through inhomogeneous cloud fields: a sensitivity study using a new stochastic cloud generator

Albert Benassi[a], Frédéric Szczap[a,*], Anthony Davis[b],
Matthieu Masbou[a], Céline Cornet[c], Pascal Bleuyard[a]

[a] *Laboratoire de Météorologie Physique, OPGC, Université Blaise Pascal, Clermont-Ferrand, France*
[b] *Los Alamos National Laboratory, Space and Remote Sensing Sciences Group, Los Alamos, NM, USA*
[c] *Laboratoire d'Optique Atmosphérique, Université des Sciences et Technologies de Lille,*
59655 Villeneuve d'Ascq cedex, France

Abstract

We analyze the effects of flat and bumpy top, fractional and internally inhomogeneous cloud layers on large area-averaged thermal radiative fluxes. Inhomogeneous clouds are generated by a new stochastic model: the tree-driven mass accumulation process (tdMAP). This model is able to provide stratocumulus and cumulus cloud fields with properties close to those observed in real clouds. A sensitivity study of cloud parameters is done by analyzing differences between 3D fluxes simulated by the spherical harmonic discrete ordinate method and three "standard" models likely to be used in general circulation models: plane-parallel homogeneous cloud model (PPH), PPH with fractional cloud coverage model (FCPPH) and independent pixel approximation model (IPA). We show that thermal fluxes are strong functions of fractional cloud coverage, mean optical depth, mean geometrical thickness and cloud base altitude. Fluctuations of "in-cloud" horizontal variability in optical depth and cloud-top bumps have negligible effects in the whole. We also showed that PPH, FCPPH and IPA models are not suitable to compute thermal fluxes of flat top fractional inhomogeneous cloud layer, except for completely overcast cloud. This implies that horizontal transport of photon at thermal wavelengths is important when cloudy cells are separated by optically thin regions.
© 2004 Elsevier B.V. All rights reserved.

Keywords: Cloud; fractal; Inhomogeneity; Radiative transfer; Infra-red; Stochastic processes

* Corresponding author. 24 Avenue des Landais, 63177 Aubiere cedex, France. Tel.: +33-3-04-73-40-73-57; fax: +33-3-04-73-51-36.

E-mail address: szczap@opgc.univ-bpclermont.fr (F. Szczap).

1. Introduction

Clouds exhibit fluctuations of optical characteristics (local extinction, effective radius, ice crystal shape) and geometrical characteristics (top bumps, gap or fractional coverage, shape or structure) at different scales. How these spatial inhomogeneities of cloud properties affect the radiative transfer is one of the major issues of atmospheric radiation theory.

Global climate models (GCMs) generally assume clouds to have constant optical properties with flat top and base: this is the plane-parallel homogeneous cloud model (PPH). In this way, two-stream approximations lead to visible radiative fluxes as functions of the cloud layer's optical depth, single scattering albedo and asymmetry parameter, whereas thermal fluxes are computed from the hypothesis that cloud layer is a "grey" body, where emissivity is function of optical depth. At best, GCM radiative transfer takes into account gaps between clouds by introducing fractional cloud coverage and linear mixing of "clear" and "cloudy" computations, where "cloudy" computations are done with optical properties that vary with wavelength (e.g. one set for each spectral band). Moreover, sensitivity studies have shown that doubling CO_2 concentration in the atmosphere produces a positive radiative forcing of 4 W/m^2 leading to an increase of 2–6 K of the surface temperature, depending on the GCM cloud parameterization. This implies radiative transfer effects of a percent or so. Since clouds play an important role in the radiative equilibrium of the earth-atmosphere system budget, cloud inhomogeneities, in addition to fractional cloud coverage, have to be taken into account in radiative transfer algorithms.

In addition to the fact that atmospheric radiative fluxes have to be accurate, their computation should be as efficient as possible. Consequently, two principal ways are proposed to take into account of cloud inhomogeneity effects in the radiative transfer. On the one hand, inhomogeneity effects are parameterized in the framework of the well established plane-parallel homogeneous cloud theory (Chandrasekar, 1960; Maedor and Waever, 1980; Lenoble, 1985). One can cite the effective thickness approximation (ETA) of Cahalan et al. (1994a), the effective homogeneous cloud approximation (EHCA) of Szczap et al. (2000a,b,c) and the other renormalization technique of Cairns et al. (2000). On the other hand, radiative transfer algorithms are proposed to take into account cloud inhomogeneities, where the main objective is the best ratio between accuracy and CPU time. One can cite the independent pixel approximation (IPA) formalized by Cahalan et al. (1994b), the Gamma-IPA by Barker et al. (1996), and, more recently, neural network techniques (Chevallier et al., 1998; Krasnopolsky and Chevallier, 2003). However, for both these approaches, cloud parameters pertinent to radiative transfer have to be identified through a rigorous sensitivity study.

Many studies point out effects of broken cloud parameters on their radiation fields in visible wavelengths (Aida, 1977; Davies, 1978; Davis et al., 1978; Gube et al., 1980; Schmetz, 1984; Kobayashi, 1993; Jonas, 1994; McKee and Cox, 1974; Bréon, 1992; Barker, 1994; Zuev and Titov, 1995). Study of cloud inhomogeneity effects at thermal wavelengths are less numerous. Some of them take into account longwave scattering processes (Takara and Ellingson, 1996), others the effects of clouds shapes and spatial distribution (Harshvardhan and Weinman, 1982; Ellingson, 1982; Killen and Ellingson, 1994; Han and Ellingson, 1999; Nasunaga and Nakajima, 2001). All these studies have used idealized clouds with cylindrical or cubic shapes. But these simple representations of

clouds are not satisfactory representations of internal fluctuations of optical depth as well as fluctuations of geometrical depth (top bumpiness) or of more realistic cloud shapes.

Some studies use clouds generated by large eddy simulations or LES (Barker et al., 1998a,b, 1999; Fu et al., 2000; Kassianov and Kogan, 2002). But their number of realizations is generally small because of a large need in memory and computational resources. Others described 3D cloud fields obtained from satellite imagery (O'Hirok and Gauthier, 1998; Chambers et al., 2001). Fractal and multifractal techniques have been used to analyze scaling and self-similarity properties of real clouds or cloud fields (Lovejoy, 1982; Cahalan, 1989; Duroure and Guillemet, 1990; Davis et al., 1994; Marshak et al., 1997; Carvahlo and Silva Dias, 1998; Gotoh and Fujii, 1998) but also in order to generate inhomogeneous (clouds) fields (Lovejoy and Mandelbrot, 1985; Schertzer and Lovejoy, 1991; Davis et al., 1991). One of the more realistic yet quite simple stochastic cloud models is the "bounded cascade" cloud model (Cahalan et al., 1994a,b; Marshak et al., 1995b). This model yields overcast horizontal fluctuations of the optical depth whose probability distribution function (PDF) is quasi-lognormal and its spectral exponent (absolute slope β of the wavenumber spectrum in log–log axes) can be made close to the frequently observed value of 5/3. But its visual aspect shows an artificial dyadic structure and, furthermore, this model does not yield broken clouds without drastic modification. Even then, the results are not compelling visually.

We therefore present a new stochastic cloud model, the tree-driven Mass Accumulation Process or "tdMAP", suitable to generate realistic overcast and broken clouds in a unique framework. Another aim is to quantify the geometrical (shape or structure, top bumpiness) and optical (fluctuations of optical depth) cloud parameters of thermal radiative fluxes in order to propose future parameterizations of cloud inhomogeneity effects in radiative algorithms in GCMs.

The organization of this paper is as follows. In Section 2, an overall picture of the tdMAP model is presented. In Section 3, it is shown how tdMAP parameters can be adjusted to generate realistic overcast and broken clouds. In Section 4, we present results of simulations of thermal radiative transfer done with spherical harmonic discrete ordinate method (SHDOM) by Evans (1998). Conditions of simulation are presented; radiative transfer simulations on top flat and bumpy one-layer cloud are shown. Comparisons are done between thermal fluxes computed with SHDOM and "approximate" radiative algorithms PPH, FCPPH and IPA. These different comparisons lead a better interpretation of the interactions between clouds and radiation. Conclusions are provided in Section 5.

2. Presentation of the tdMAP model

Simulation of complex media is a pressing problem and a challenging one. Clouds are examples of such a task. The media we are interested in are inherently random. So, in this context, a medium can be seen as a realization of a stochastic process. We shall use a parameterized model, in such a way as to make a given type of signal or field correspond a given set of parameters.

Our objective here is to simulate 2D horizontally optical depth fluctuations of overcast and broken cloud field. Clouds exhibit fluctuations of their microphysical and macro-physical properties at different (averaging) scales. The cloud-radiation community traditionally distinguishes two kinds of cloud inhomogeneities: "geometrical inhomogeneity" (gaps between clouds showing different shapes or structures, cloud top bumps) and "internal inhomogeneity" characterized by fluctuation of optical properties (extinction, effective radius, etc.) inside the cloud.

The "internal" cloud fluctuations show a scale-invariant regime, defined by the range of scales where wavenumber spectra and other spatial statistics follow powers laws. Davis et al. (1994, 1996) estimated this range for three specific stratocumulus events: a few meters to a few tens (possibly of) kilometers, with an absolute spectral slope $\beta = 1.1 - 1.7$. At smaller scales (down to about 4 cm), Davis et al. (1999) found enhanced variability of liquid water content in clouds that was traced by Jeffery (2001) to inertial effects in the small-scale turbulence. The lower limit is in fact not defined due to the limited resolution of the instruments. The theoretical lower limit is molecular dissipation scale of a few millimeters or larger, depending of the turbulence intensity. On the other hand, the upper limit of this range (low frequency) defines the "integral scale" where the spectrum becomes flat (decorrelation occurs). This "integral scale" varies from one cloud field to another. For example, Cahalan and Snider (1989) found that wavenumber spectrum $E(k)$ of liquid water path in marine stratocumulus follows a power law from about 500 km to somewhat less than 500 m from satellite data analysis. The 500-m break is, however, an apparent effect due to cloud-radiation interactions called "radiative smoothing" (Marshak et al., 1995a; Davis et al., 1997). In our work, the lower limit will be the cloud pixel size, and the upper limit, or the "integral scale", will be close to the horizontal extent of our synthetic clouds. Therefore, the "integral scale" is limited by our computation resources (CPU time and memory size) when radiative transfer simulations are running.

The statistical theory of turbulence proposed by A. Kolmogorov was the departure of an enormous amount of work. Let us refer to Frisch (1995) for a complete exposition. Supporting directly or inspired by this progress in turbulence theory, two kinds of models were proposed: first, the multiplicative cascade model (Kolmogorov, 1962; Novikov and Stewart, 1964) and then Fractional Brownian Motions or FBMs (Mandelbrot and Van Ness, 1968). Our model, called "tree-driven mass accumulation process" (tdMAP), pays tribute to those both classes of mathematical models.

We start with a wavelet like decomposition of the FBM (Benassi, 1995) we shall call a multiresolution analysis. Self-similar properties are a main feature in Komogorov theory. FBM, which we denote $X(x)$ enjoys this property, which is expressed by the equation

$$(X(\lambda x))_{x \in R^D} \triangleq (\lambda^H X(x))_{x \in R^D} \tag{1}$$

where $\triangleq$ is the statistical equality, x is the spatial position, λ is the scale, $D = 1,2,3$ is the spatial dimension and H is the so-called Hurst parameter ($H = 1/2$ for Brownian motion). Following Benassi (1995), Benassi et al. (1997) and Benassi and Deguy (1999), we obtain the wavelet decomposition of the FBM, given by

$$X(x) = \sum_{\lambda \in \kappa_D} 2^{-|j|H} \phi_{\lambda_H} \xi_\lambda \tag{2a}$$
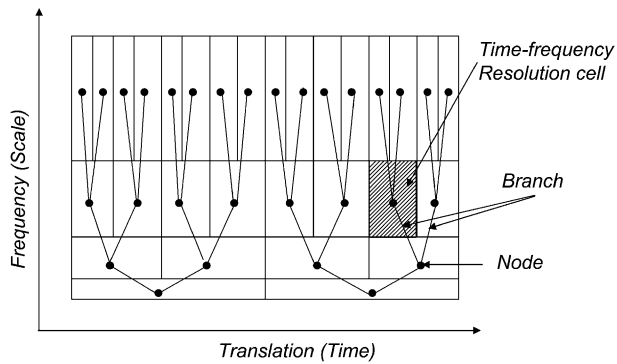
Fig. 1. Time-scale resolution of wavelet transforms and the ≪tree-structure≫ extracted from it. This ≪tree≫ is composed of nodes (points on the figure) from which leave branches (two in this case). To each time-frequency resolution cell correspond a node of the tree.
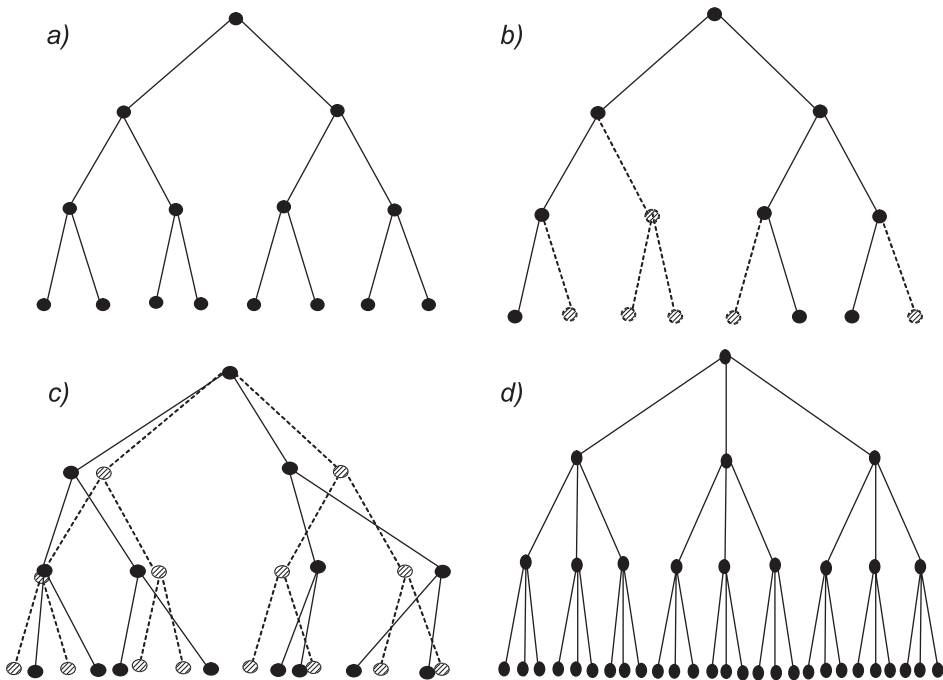

Fig. 2. Example of imposed "tree-structure" modified by (p, q, b) "action" parameters. Number of cascades: $j = 3$. (a) "Classical" tree-structure: all nodes and branches are kept ($p = 1$) and from each node leave two branches (partition parameter $b = 2$). (b) At each node, branches (and sub-nodes and sub-branches) are pruning with probability $p < 1$. Pruned branches and nodes are dotted and hatched respectively. (c) Effect of random spatial shift of each node on the general "tree-structure". Original and "random shifted" tree are respectively dotted et solid line. (d) Example of tree structure with "branching" rate $b = 3$: from each node leave three branches.
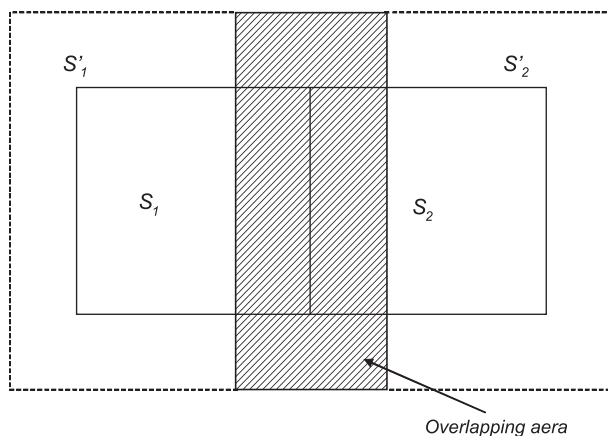
Fig. 3. Explanation of "overlapping" process.

with

$$\phi_{\lambda_H}(x) = \phi_H(2^j x - k). \tag{2b}$$

It is *optimal*, because ξ_λ is a family of independent and identically distributed normal random variables. Function ϕ_H is specific to each value of H. κ_D is the 2^D-adic net (see Fig. 1,
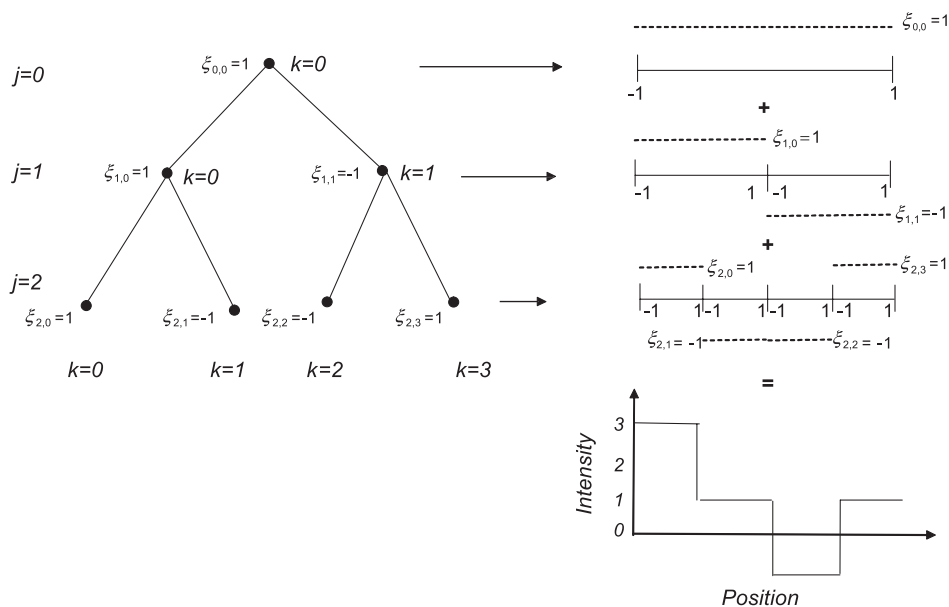

Fig. 4. Explanation of the generation of 1D simple signal with tdMAP model ($H=0$, $F=1$, $\xi=1$ or -1, $b=2$, $p=1$, $j_{max}=2$, $q=0$). One begins by defining a "tree structure". On each node of the tree, at position k and scale j, are defined the "masses" (function F, random variable ξ, Hurst parameter H) and the "actions" (Bernoulli parameter p, "branching" rate b). Finally, one sums of the mass along the tree to generate the signal.

where "positions" k are contingent on "scale" j). Furthermore, κ_D may be seen as a tree or arborescence. This tree naturally encodes points in the space (j, k) of the phenomenon.

But, at the same time, we can "decorate" (just like a Christmas tree) each of its nodes (j, k) with different "objets" and "actions" (generally mathematically identifiable). This tree κ_D allows us to take into account the cascade phenomenon. This new framework leads us to present the basic form of tdMAP model as a generalization of the wavelet decomposition of above FBM; tdMAP model can thus be written as

$$X(x) = \sum_{\lambda \in T_p} 2^{-jH_\lambda} F_\lambda(x) \xi_\lambda. \tag{3}$$

If κ_D is the preceding tree, $j \in N$ is the height in κ_D of the node $\lambda = (j, k)$ and $k \in Z^D$ are integer-valued vectors. k corresponds to the spatial position $x = k/2^j$, corresponding to node λ. Now T_p is a random sub-tree of κ_D determined by the parameter p (definition of p further in the text). F is called the "morphlet" and commonly here, $F_\lambda(x) = F(2^j x - k)$; ξ_λ are random variables; H_λ is now a *local* Hurst parameter, commonly taken as a constant here.

Let us give more details on the tdMAP parameters. T_p is a "pruned" tree. The "pruning" is due to a Bernoulli (with parameter p) percolation on κ_D. We recall that the Bernoulli distribution is a discrete distribution having two possible outcomes labeled $\eta = 0$ and $\eta = 1$ in which $\eta = 1$ ("success") occurs with probability p and $\eta = 0$ ("failure") occurs
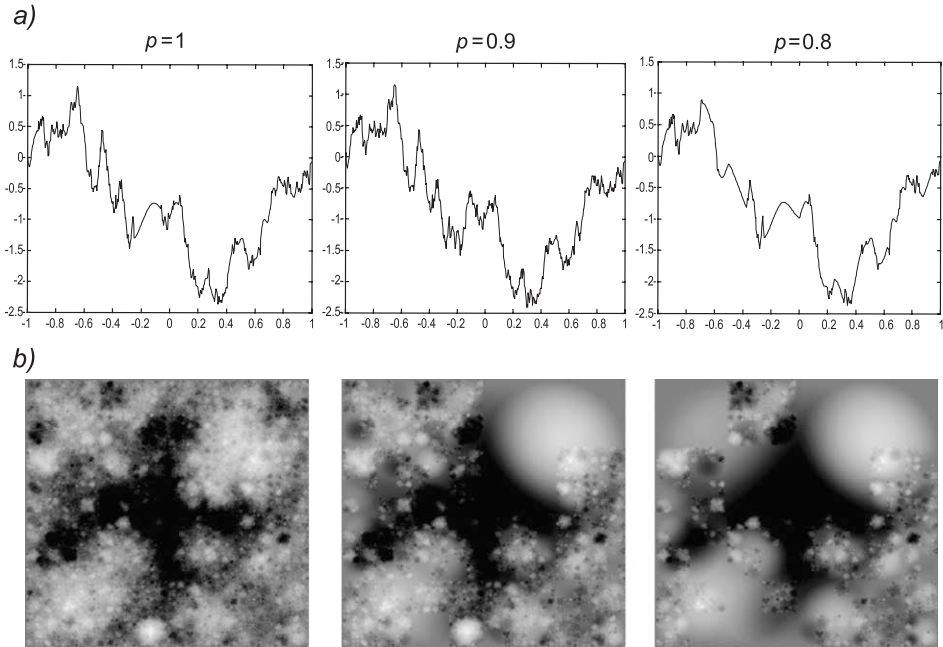

Fig. 5. (a) Illustration of the tdMAP model for tree values of Bernoulli parameter p (1, 0.9 and 0.8, respectively). Hurst parameter is set to $H = 0.5$ and space dimension $D = 1$. For $p = 1$, it is indistinguishable from fractional Brownian motion (Benassi et al., 1997). (b) Same as Fig. 3a, but space dimension $D = 2$. The basic shape of the morphet (a Gaussian) can be seen clearly at the largest scales and the smallest p.

with probability $1 - p$, where $0 \leq p \leq 1$ is the Bernoulli parameter. If $p = 1$, all nodes and branches of the tree are kept (see Fig. 1a). If not, each branch is removed with probability $1 - p$. The Bernoulli parameter thus allows us to generate fractional cloud coverage without using an ad hoc threshold technique (see Fig. 2b).

To better simulate cloud fields, we need some enrichments. So we add new "objets" and "actions" on the nodes of T_p. We define action S_q where parameter q indicates the intensity of the action. For example, action S_q can control how the support of the morphlet F is horizontally shifted. Let us give the definition of the support of the morphlet F. Let Ω be the definition domain of the morphlet F: $\Omega = [-1, 1]^D$, where D is the space dimension. If $D = 2$, $F(x,y):\mathbb{R}^2 \to \mathbb{R}$. Let Supp($F$) be the support of the morphlet F. Supp(F) is the set of all points (x, y) which satisfy the condition $|F(x, y)| > 0$. For example, $q = 1.5$ implies morphlet F is randomly and independently shifted by its support diameter times 1.5. It is interesting to control how the support of the morphlet F is horizontally shifted in order to remove the dyadic structure of the simulated signal (Fig. 2c).

If Supp(F) $\subset \Omega$, there is "no overlapping", which is one condition in the present paper. But in general case, Supp(F) $\not\subset \Omega$, and leads to an "overlapping" process. The overlapping process consists in dilating the support of morphlet F at node $\lambda = (j, k)$ (see Fig. 3). This action gives smoother simulated signals.

Now let us briefly explain how to realize a broken cloud field with fractional cloud coverage C, where C is cloudy area in percent. It can be done in different ways, most notably by modifying the geometry of the tree. For example, we can modify the "branching" rate
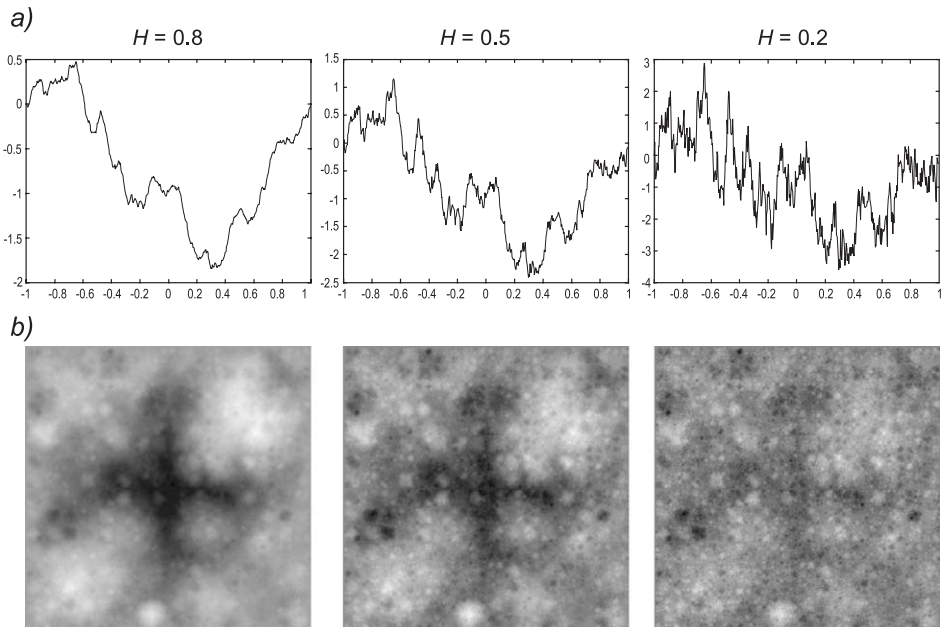

Fig. 6. (a) Illustration of the tdMAP model for tree values of Hurst parameter H (0.8, 0.5 and 0.2, respectively). Bernoulli parameter is set to $p = 1$. (b) Same as Fig. 4a, but space dimension $D = 2$.

from the scale 0 to the "geometry" scale J_0, with morphlet F is set to the null function. Let b be the "branching" rate. The "branching" rate is the number of branches leaving form one node of the tree (on Fig. 2a and d, $b = 2$ and $b = 3$, respectively). C can be expressed as

$$C = \frac{p^{J_0} b^{J_0 D}}{b^{J_0 D}} = p^{J_0}, \tag{4}$$

where p is the Bernoulli parameter, b the "branching" rate, D the space dimension and J_0 the "geometry" scale. The control of the geometry of the tree with the help of the branching number leads to control the cloudy areas number for a given fractional cloud coverage C
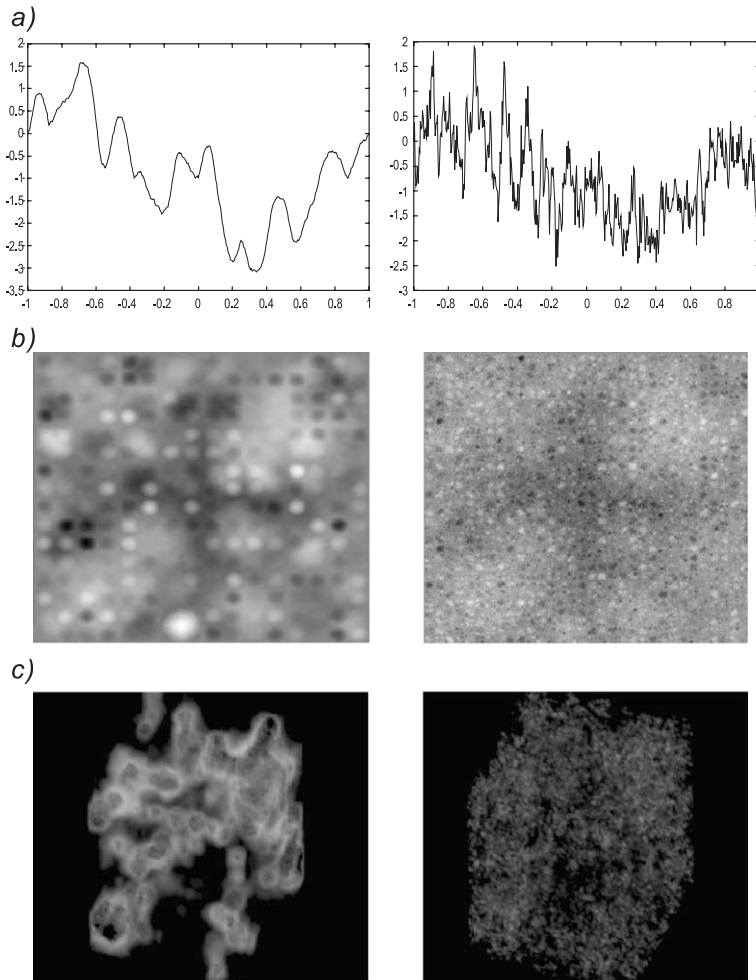

Fig. 7. Illustration of generalized fractional Brownian motion. Bernoulli parameter $p = 1$. H is now a function of scale ($H_{0 \leq \text{scale} < 4} = 0.2$ and $H_{4 \leq \text{scale} < \infty} = 0.8$ for left pictures and $H_{0 \leq \text{scale} < 4} = 0.8$ and $H_{4 \leq \text{scale} < \infty} = 0.2$ for right pictures). (a) Space dimension $D = 1$. (b) Space dimension $D = 2$. (c) Space dimension $D = 3$. The 3D pictures are obtained by tomographic projection of the 3D field.

imposed by p. So, for scales from 0 to J_0, we are basically punching holes in the cloud cover; for scales $j > J_0$, we will be generating internal cloud structure. For this, we need "objects".

Now, we focus on the objects deposited along the tree-structure T_p we want to work with (i. e. where we have not already applied null values). These objets are the function F, the random variables ξ and the value of the Hurst parameter H. Since the optical depth distribution of cloud field is, by essence, positive value, morphlet F and random variables ξ must be positive. Fig. 4 shows the building of a very simple 1D (one dimension) signal ($H = 0$, $F = 1$, $\xi = 1$ or -1, $b = 2$, $p = 1$, $j = 2$). One begins at the scale $j = 0$ and multiplies the morphlet F defined on its support $[-1,1]$ by the random variable ξ. Then one defines two nodes at the scale $j = 1$. For each node is defined the scaled function F on its scaled compact support. The above process is repeated iteratively until the final scale. In doing so, we have defined a weighed value on each position on the tree. Finally, one makes the sum of the weight mass along the tree branches to generate the final simulated signal.

Figs. 5–7 show some tdMAP signals generated in very general cases.

3. Choice of tdMAP parameters to generate stratocumulus and cumulus clouds fields

3.1. Stratocumulus field

The objective, in this section, is to generate horizontal 2D optical depth fields (x–y axes), with uniform (optical and geometrical) properties along the vertical (z-axis). Table 1 gives the "ad hoc" tdMAP model parameters values to generate 2D (256×256 pixels) synthetic stratocumulus cloud fields sharing statistical properties with those of real stratocumulus fields. Number of cascade steps is set to 8 ($2^8 = 256$). Self-similarity properties of stratocumulus field from the upper to the lower scale are conditioned by the Hurst parameter H. The relation between the Hurst parameter H and the absolute value of the spectral slope β of the wavenumber spectrum in log–log axes is given by

$$\beta = 2H + 1 \tag{5}$$

Therefore, H is set to 0.25 in order to impose an absolute spectral slope of 1.5. Moreover, since optical depth is a positive quantity, random variables ξ_λ and functions F_λ must be positively valued.

Table 1
tdMAP model parameters values to generate synthetic stratocumulus fields (see Section 3.1 for more explanations)

Scale	Objects			Actions		
	F	ζ	H	b	p	q
0	F_1	–	–	5	1	0
1	F_1	e^u	0.25	2	1	0.2
2	F_1	e^u	0.25	2	1	0.3
3	F_1	e^u	0.25	2	1	1.5
⋮	⋮	⋮	⋮	⋮	⋮	⋮
8	F_1	e^u	0.25	2	1	1.5

The choice of function F_1, given by

$$F_1(x,y) = \exp(-(x^2/\sigma^2 + y^2/\sigma^2)) \qquad (6)$$

is guided by the fact, on the one hand, this function yields theoretical results (which is the focus of a future work), and on the other hand, standard deviation σ can be modulated and was set for the present study to 2.5. This makes the cloud edges appropriately fuzzy at the smallest scale. Random variables ξ follow specific "log-uniform" law defined by taking the exponential of a uniform variable u on $[-1,1]$. The tdMAP model is a summation process and synthetic optical depth distribution is in this case close to a log-normal distribution as is often observed in real stratocumulus fields (Cahalan et al., 1994a). Moreover, this specific law enables us to avoid too extreme values of the optical depth.

Spatial shift parameter q is varied from 0 to 1.5, as a function of scale (we recall this means "morphlet" F_1 is randomly and independently shifted by its support diameter times 1.5 if S_q=.5). The main advantage of the parameter q is to eliminate the artificial dyadic structure, without significantly changing the absolute spectral slope β.

3.2. Cumulus fields

Let us focus now on how generate fractional cloud coverage. Table 2 gives the "ad-hoc" tdMAP model parameters values to generate 2D (256×256 pixels) synthetic cumulus cloud fields. Traditionally, one simulates overcast cloud fields with a stochastic process and has recourse to a threshold to generate partial cloud coverage. In the tdMAP framework, the cloud coverage generation process is reversed. Firstly, at scale 0, we imposed the null morphlet with the Bernoulli parameter set to $p=0.5$ if the desired could coverage is $C=0.5$ (50% of the tree structure is destroyed). Then, the process explained above for stratocumulus generation in Section 3.1 is re-done the first scale ($j=1$) toward the finest scale $j=8$, with

Table 2
tdMAP model parameter value to generate synthetic cumulus fields with partial cloud coverage (see Section 3.2 for more explanations)

Scale	Objects			Actions		
	F	ζ	H	b	p	q
0	0	–	–	5	0.5	0
1	F_2	e^u	0.25	2	1	0.2
2	F_2	e^u	0.25	2	1	0.3
3	F_2	e^u	0.25	2	1	0.3
4	F_2	e^u	0.25	2	1	0.3
5	F_1	e^u	0.25	2	1	1.5
$\vdots$	$\vdots$	$\vdots$	$\vdots$	$\vdots$	$\vdots$	$\vdots$
8	F_1	e^u	0.25	2	1	1.5

Bernoulli parameter $p = 1$. However, from the scale 1 to the scale 4, the function F_2 is used given by

$$\begin{cases} F_2(x,y) = (x^2 - 1)(y^2 - 1) & \text{if } x^2 + y^2 \leq 1 \\ F_2(x,y) = 0 & \text{if } x^2 + y^2 \geq 1 \end{cases} \tag{7}$$

Therefore, cloud edges are smooth and clean at the largest scales.

3.3. Examples of tdMAP clouds

Figs. 8 and 9 show 2D horizontal fluctuations of optical depth of an overcast and broken cloud fields, respectively. SHDOM computations at 0.55 μm wavelength for nadir
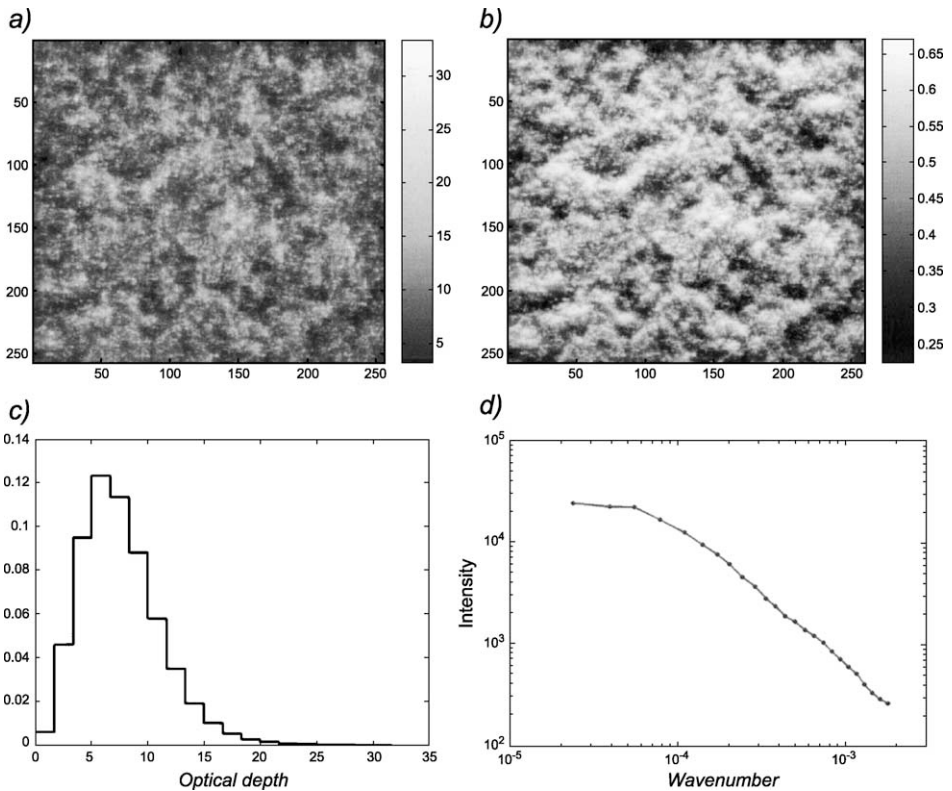
Fig. 8. (a) Example of overcast 2D optical depth field generated with tdMAP (mean optical depth = 10) and (b) its normalized visible radiance fields simulated with SHDOM (solar angle $\theta_0 = 45°$, nadir angle view, cloud base = 0.5 km, mean geometrical depth = 300 m, pixel size = 12.5 m). The probability density function (PDF) is represented in (c). Power spectrum in Fourier space is showed in (d) and estimated spectral slope is $\beta = 1.5$ below the integral scale of 1 km where the slope goes from flat to decreasing. The spectrum becomes flat at the lower limit because "branching" parameter n is set to 5 at the scale 0.
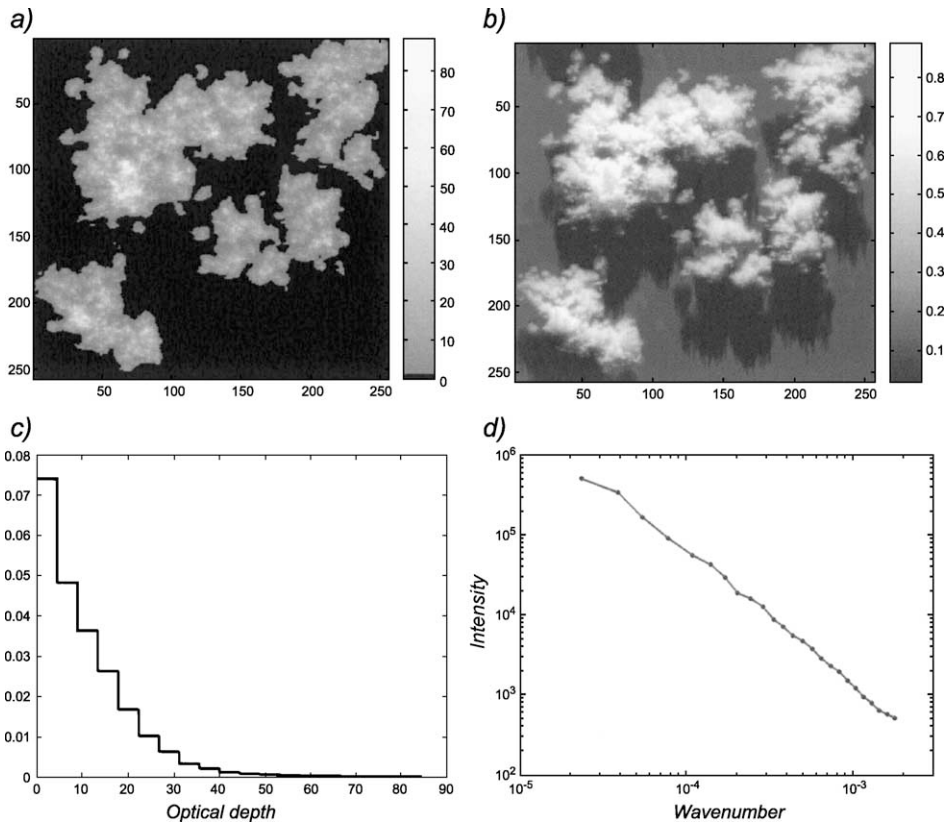
Fig. 9. (a) Example of broken 2D optical depth field generated with tdMAP (mean overall optical depth = 5) and (b) its normalized visible radiance fields simulated with SHDOM (conditions of simulations same as Fig. 5). The probability density function (PDF) is represented in (c). Power spectrum in Fourier space is showed in (d) and estimated absolute spectral slope is $\beta = 1.7$.

radiances and solar illumination from $45°$ are also shown. Finally, two key statistical properties are plotted (one-point PDF and wavenumber spectrum).

4. Effects of inhomogeneous clouds on thermal radiative fluxes

4.1. Conditions of radiative transfer and inhomogeneous clouds simulations

The main objective of the present study is to evaluate the effects of pertinent cloud parameters on thermal radiative fields. Radiative transfer simulations are done with the SHDOM algorithm (Evans, 1998) and a correlated k-distribution (Fu and Liou, 1992). The U.S. standard atmosphere is assumed. Concentration of CO_2, CH_4 and NO_2 are set to 330, 1.7 and 0.31 ppmv, respectively. Surface emissivity is set to unity; its temperature is set to 288.1 K. Main SHDOM parameters are: convergence criteria (10^{-4}), discrete ordinates

$(N_\mu, N_\varphi = 16)$, cloud spatial resolution $(N_x = 128, N_y = 128, N_z = 60)$, so the "adaptive grid" option is not used. Following Evans (1998), the error in absolute fluxes is less than 1%.

The 2D (128×128 pixels) tdMAP cloud fields have horizontal extension of 64×64 km. Each 0.5×0.5 km cloud pixel is assumed to be vertically homogeneous up to a cloud top height which is either held constant or varied with optical depth (as explained further on). This pixel scale is considerably larger than in Figs. 5b and 6b but enables the outer scale of 64 km to be commensurate with pixel size of GCMs (even though finest cloud structures are not well resolved and therefore small scale cloud inhomogeneity effects are not taken into account). Cloud temperature is assumed equal to atmospheric temperature. Variable cloud parameters are cloud base altitude ($Z_b = 1$, 4 km), mean or constant geometrical thickness ($h = 0.5$, 1, 2, 4 km), mean optical depth ($\bar{\tau} = 2$, 5, 10, 20), fractional cloud coverage ($C = 0.25$, 0.58, 1). The distribution of cloud droplet size of is assumed to be log-normal with log-standard deviation of 0.35 (Nakajima and Nakajima, 1995). Effective radius is set to 10 µm. Fig. 10 shows the structure of three optical depth field structure with overall (cloud + clear) mean optical depth equal to 5. Hereafter, they are called Cl1, Cl2 and Cl3, respectively.
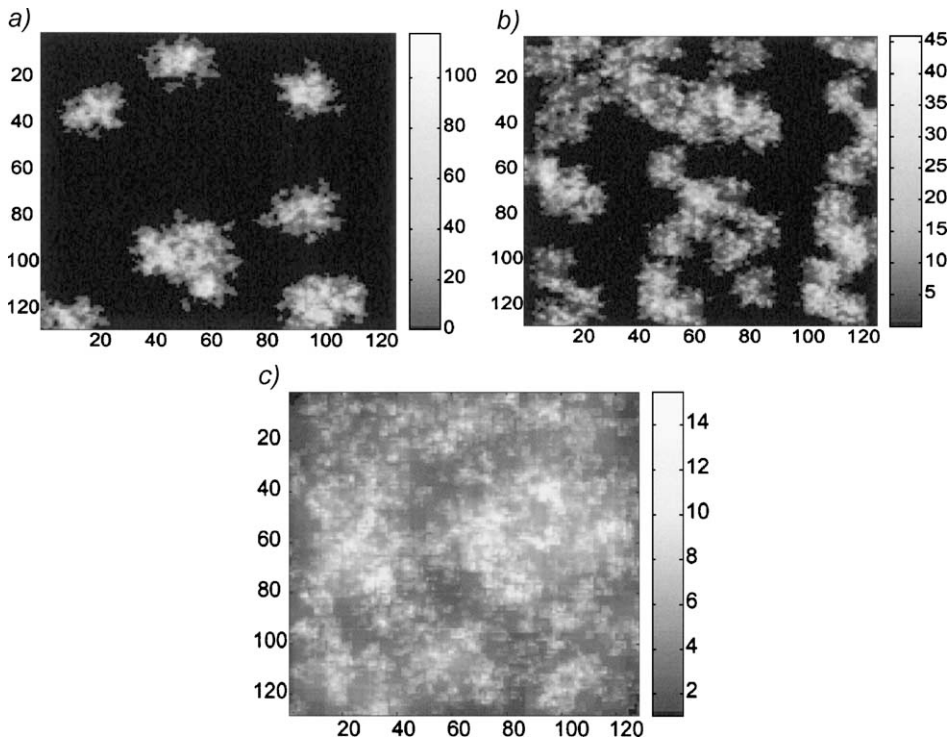

Fig. 10. Three optical depth fields (mean optical depth $\bar{\tau} = 5$) generated with tdMAP with different fractional cloud coverage: (a) Cl1, $C = 0.25\%$, (b) Cl2, $C = 0.58\%$ and (c) Cl3, $C = 100\%$.

In order to determine which cloud parameters are pertinent to thermal radiative transfer, with the intention to interpret cloud-thermal radiation interactions, we compute differences (or biases) between domain-average fluxes computed from 3D SHDOM model, considered as the benchmark, and from the "standard" approximate methods PPH, plane-parallel homogeneous with fractional cloud (FCPPH) and IPA methods. These biases are written $\delta F_{\text{Direction}}^{\text{3D-approx}}$, where Approx = PPH, FCPPH or IPA, and Direction = up or down. Note that where *up* indicates the bias estimated far above the cloud layer (altitude = 20 km) for flux going into space, and *down* indicates the bias estimated below the cloud layer (altitude = 0 km) for fluxes going into ground. $\delta F^{\text{3D-PPH}}$ is due to the plane-parallel bias (Cahalan et al., 1994a), fractional coverage and net horizontal transport of photons (Cahalan et al., 1994b; Titov, 1998; Marshak et al., 1995a,b; Faure et al., 2001a,b). $\delta F^{\text{3D-PPH}}$ is mostly due to the plane-parallel bias and net horizontal transport of photons. $\delta F^{\text{3D-IPA}}$ is only due to the net horizontal transport of photons, which, beyond cloud fraction, is largely controlled by the *horizontal* optical thickness τ of cloud cells; on average this is $\bar{\tau}_{\text{cell,hor}} = \bar{\tau}(0.5/h)$ for h in km. The smaller $\bar{\tau}_{\text{cell,hor}}$, the larger the net horizontal fluxes.

So we are using 3D SHDOM model as the point of reference rather than the simplest (PPH) approximation. This departs from tradition in 3D radiative transfer studies but has the advantage of highlighting the potential GCM modeling error.

Simulations of thermal radiative transfer should be done in the complete [4–100] μm wavelength interval. But we preferred to compute thermal radiative fluxes in the [10.2–12.5] μm interval for two reasons. The first is to reduce computation time. The second is because gas absorption is minimal for the atmospheric window. Therefore, cloud effects are dominant for this wavelength interval and consequently thermal clouds inhomogeneities effects in the [10.2–12.5] μm band are the most representative of those in the full [4–100] μm interval (Takara and Ellingson, 1996).

4.2. Flat top cloud case

Fig. 11 shows $\delta F_{\text{up,down}}^{\text{3D-PPH}}$ and $\delta F_{\text{up,down}}^{\text{3D-IPA}}$ for the cloud Cl1 and for two cloud base altitude ($Z_b = 1, 4$ km). $\delta F_{\text{up,down}}^{\text{3D-PPH}}$ is larger than $\delta F_{\text{up,down}}^{\text{3D-IPA}}$ within a ratio of around 10 and reaches a maximum of ± 1 W/m^2. This implies, as for solar wavelengths (Cahalan et al., 1994b) but, in a slighter way, plane-parallel bias is not negligible. On the other hand, $\delta F_{\text{up,down}}^{\text{3D-IPA}}$ is very small (max of $\delta F_{\text{up,down}}^{\text{3D-IPA}} = \pm 0.3$ W/m^2), so we can assume the IPA method is suitable to compute thermal radiative fluxes of overcast and flat top inhomogeneous clouds.

This implies also that horizontal transport of photon for overcast and flat top inhomogeneous clouds is negligible for thermal wavelengths. As expected, the level curves for IPA biases roughly follow lines of constant values for $\bar{\tau}_{\text{cell,hor}}$ (with lower values for higher $\bar{\tau}_{\text{cell,hor}}$).

Fig. 12 shows $\delta F_{\text{up,down}}^{\text{3D-PPH}}$, $\delta F_{\text{up,down}}^{\text{3D-FCPPH}}$ and $\delta F_{\text{up,down}}^{\text{3D-IPA}}$ for the cloud Cl2 and for two cloud base altitude ($Z_b = 1, 4$ km). Whatever are the cloudy conditions, $\delta F_{\text{up,down}}^{\text{3D-PPH}}$ are quite large (max of $\delta F_{\text{up,down}}^{\text{3D-PPH}} = \pm 16$ W/m^2) and they are of a constant sign that is easily explained by the direct visibility (through holes) of (warm) ground from space and (cold) space from ground. $\delta F_{\text{up,down}}^{\text{3D-FCPPH}}$ and $\delta F_{\text{up,down}}^{\text{3D-IPA}}$ are of same magnitude (max of $\delta F_{\text{up,down}}^{\text{3D-PPH}}$ or $\delta F_{\text{up,down}}^{\text{3D-IPA}} = \pm 5$ W/m^2) but smaller than $\delta F_{\text{up,down}}^{\text{3D-PPH}}$. It can be noticed that $\delta F_{\text{up,down}}^{\text{3D-IPA}}$ is always positive and $\delta F_{\text{up,down}}^{\text{3D-PPH}}$ is always negative (the opposite of their "3D-PPH"
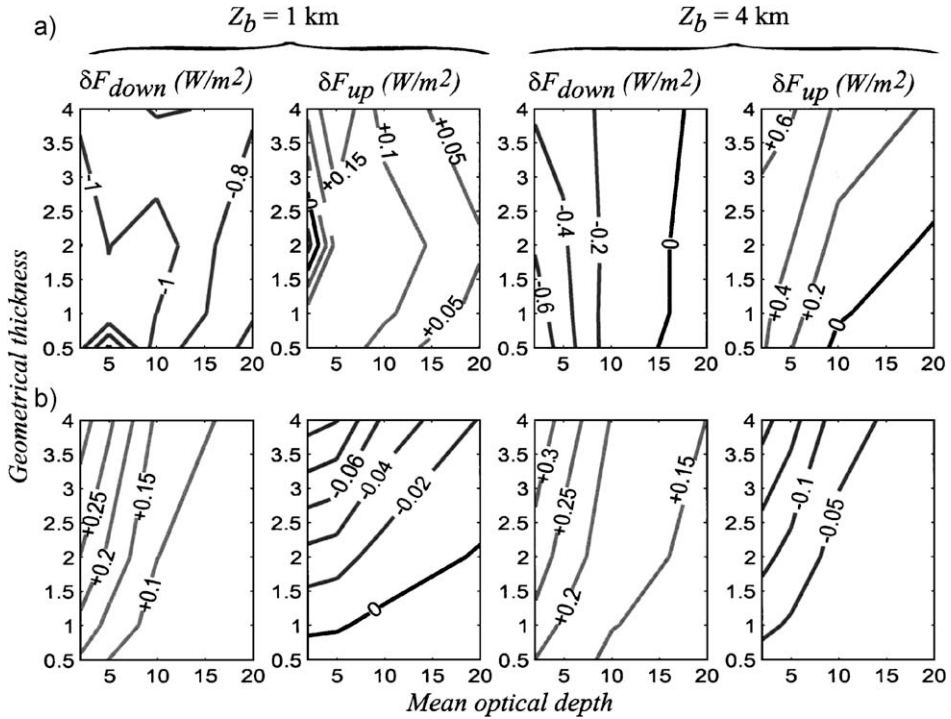
Fig. 11. Contour of $\delta F_{up,down}^{3D-approx}$ (a) Approx = PPH, (b) Approx = IPA for cloud Cl3 (fractional cloud coverage $C = 100\%$), as a function of mean optical depth and geometrical thickness. Two cloud base altitudes are represented: $Z_b = 1$ km and $Z_b = 4$ km. See text for more explanation.

counterparts) whereas $\delta F_{up,down}^{3D-FCPPH}$ can be positive or negative and even equal to zero within particular conditions (see Fig. 12(b)).

This implies that IPA and FCPPH methods can take into account of effects of gaps between clouds only in a limited way and tend to over compensate the 3D effects. Therefore, and because $\delta F_{up,down}^{3D-FCPPH}$ and $\delta F_{up,down}^{3D-IPA}$ are roughly equal in magnitude, $\delta F_{up,down}^{3D-FCPPH}$ and $\delta F_{up,down}^{3D-IPA}$ are principally explained by horizontal transport of photons between clouds but not for "internal horizontal fluctuation" of optical depth. For cloud coverage of 50%, these results let us conclude that PPH method is not at all adapted to compute fluxes of fractional inhomogeneous flat-top clouds. Moreover, and even through FCPPH and IPA methods provide better results than PPH method, they are not sufficiently accurate methods to take account of fractional clouds inhomogeneities in thermal wavelengths. Indeed, cloud boundaries with clear areas drive significant horizontal fluxes that only the full 3D calculation account for.

Fig. 13 shows $\delta F_{up,down}^{3D-PPH}$, $\delta F_{up,down}^{3D-FCPPH}$ and $\delta F_{up,down}^{3D-IPA}$ for the cloud Cl3 ($C = 25\%$) and for two cloud base altitude ($Z_b = 1, 4$ km). Whatever are the cloudy conditions, $\delta F_{up,down}^{3D-PPH}$ is very large (max of $\delta F_{up,down}^{3D-PPH} = \pm 28$ W/m^2). $\delta F_{up,down}^{3D-FCPPH}$ and $\delta F_{up,down}^{3D-IPA}$ are of same magnitude (max of $\delta F_{up,down}^{3D-FCPPH}$ or $\delta F_{up,down}^{3D-IPA} = \pm 3$ W/m^2) but are smaller than $\delta F_{up,down}^{3D-PPH}$. Our conclusions for cloud Cl2 carry over to cloud Cl3 unchanged.
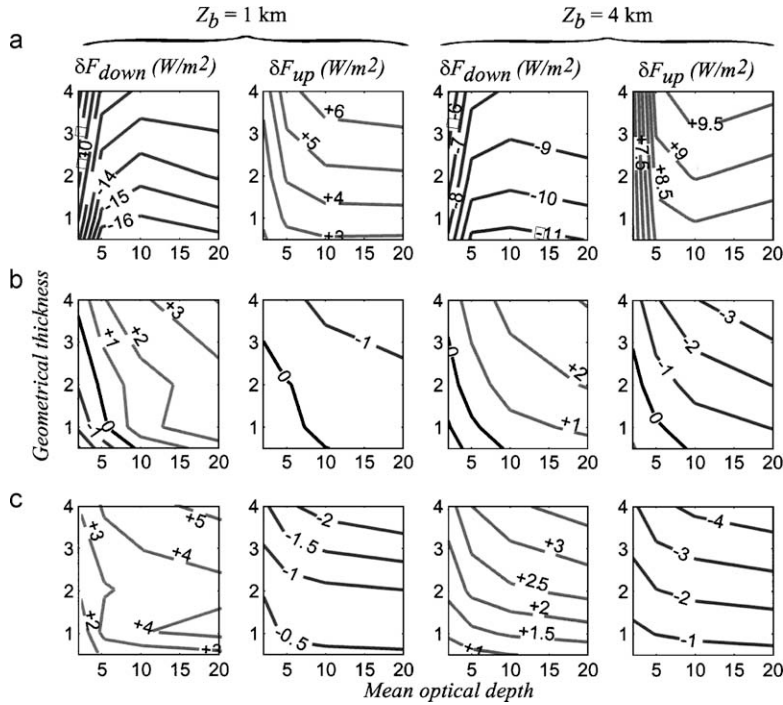
Fig. 12. Same as Fig. 10 but (a) Approx. = PPH, (b) Approx = FCPPH and (c) Approx. = IPA bias and for cloud Cl2 (fractional cloud coverage $C = 58\%$).

These results show, unsurprisingly, that the smaller the fractional cloud coverage, the less accurate the PPH method becomes. They also show that FCPPH and IPA methods are not adapted for fractional inhomogeneous flat top cloud (except for overcast cloud), even if accuracy of both these methods does not depend on the cloud coverage parameter. Figs. 11–13 also exhibit, in addition to the cloud coverage parameter, what cloud parameters are pertinent to radiative transfer. As for visible wavelengths, optical depth is an important parameter. One can notice that $\delta F_{up,down}^{3D-PPH}$, $\delta F_{up,down}^{3D-FCPPH}$ and $\delta F_{up,down}^{3D-IPA}$ are not only strong functions of optical depth (biases are very sensitive to optical depth when optical depth is smaller than 10) but also to geometrical thickness. This is clearly a cloud emissivity effect. Generally, the larger geometrical thickness is, the larger are the values of $\delta F_{up,down}^{3D-PPH}$, $\delta F_{up,down}^{3D-FCPPH}$ and $\delta F_{up,down}^{3D-IPA}$ This is the effect of thermal gradients inside the thicker clouds since as h increases (for given $\bar{\tau}$) extinction goes down and photons will tend to originate from deeper inside the cloud.

4.3. Bumpy cloud top case

Cloud base can generally be considered flat. On the other hand, cloud top is rather bumpy, even through in stratocumulus at an inversion, the cloud base can be more variable than the cloud top. Not many papers deal with relationships between top and base cloud
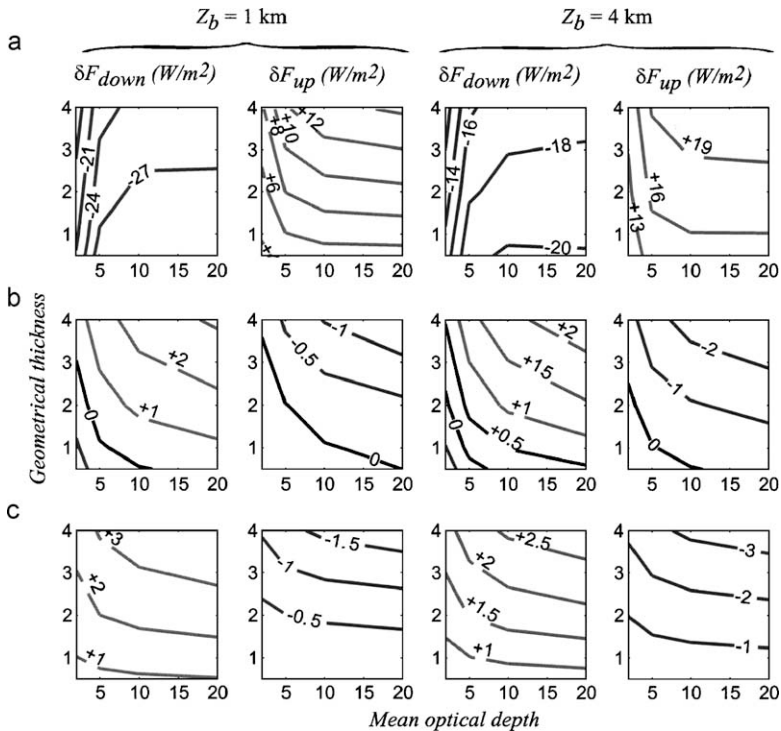
Fig. 13. Same as Fig. 10 but for cloud Cl1 (fractional cloud coverage $C = 0.25\%$).

height and their optical properties. Albrecht et al. (1990) demonstrated that, for the adiabatic approximation for shallow layers, liquid water path (LWP) is proportional to the square of the layer thickness. Minnis et al. (1992) observed same result by least-squares regression fit to their data. As a first approximation (constant effective radius assumption), optical thickness is proportional to the LWP. Therefore, we propose to prescribe cloud geometrical thickness $h_{i,j}$ of each pixel (i,j) by

$$h_{i,j} = H_0 \left(\frac{\tau_{i,j}}{\tau_{max}} \right)^\alpha$$

where $\tau_{i,j}$ is the optical depth of pixel (i,j), τ_{max} the maximum of the cloud field optical depth, α is an exponent and H_0 is a constant value computed in such a way that mean geometrical thickness of bumpy cloud equals geometrical thickness of the corresponding flat-top cloud. Effects of clouds-top bumps are studied for two values of the α exponent, $\alpha = 0.5$ (distribution 1) proposed by Albrecht et al. (1990) and Minnis et al. (1992) and $\alpha = 0.7$ (distribution 2) proposed by Barker et al. (1998a,b). Fig. 14 shows geometrical thickness histogram of bumpy cloud Cl2 with mean geometrical thickness equals 2 km. From the same optical depth field (here cloud Cl2), distribution 2 of geometrical thickness is less concentrated around the mean geometrical thickness than distribution 1. We
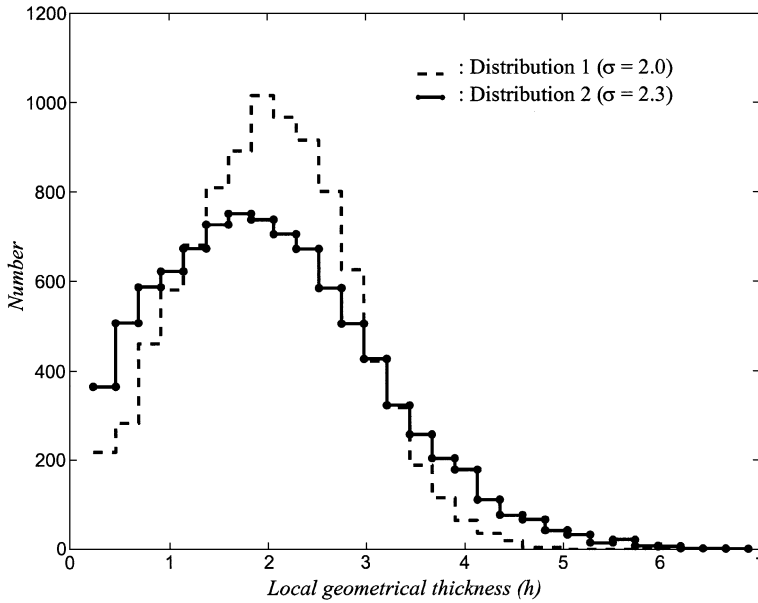
Fig. 14. Geometrical thickness histogram of bumpy cloud Cl2 ($C = 0.58\%$). Mean geometrical depth $\bar{h} = 2$ km. Distributions 1 and 2 correspond to $\alpha = 0.5$ and $\alpha = 0.7$, respectively.

therefore expect larger radiative effects for cloud bumps generated with distribution 2 than with distribution 1.

Fig. 15 shows absolute bias $\delta F_{\text{up,down}} = F_{\text{up,down}}^{\text{bumpy top}} - F_{\text{up,down}}^{\text{flat top}}$ between 3D SHDOM fluxes of bumpy and flat top clouds, as a function of mean optical depth and mean geometrical thickness for distribution 2 ($\alpha = 0.7$), for two cloud base altitudes ($Z_b = 1$, 4 km) and cloud Cl2 ($C = 0.58\%$). As expected, $\delta F_{\text{up,down}}$ are larger for distribution 2 than for distribution 1 (not shown). These biases are, as a whole, rather small ($F_{\text{up,down}} < 0.5$ W/m^2), except for F_{up} with mean geometrical thickness larger than 1 km ($\max(|\delta F_{\text{up}}|) = 4$ W/m^2).

$\delta F_{\text{up,down}}$ for cloud Cl1 and Cl3 are not shown but they are not larger than $F_{\text{up,down}}$ for Cl2. One can conclude that effects of cloud bumps are, as a whole, relatively small for thermal radiative transfer. Therefore, thermal radiative properties of inhomogeneous bumpy top clouds can be well approximated by inhomogeneous flat top cloud as long as the mean geometrical thickness is not larger than 1 km. But we must remember that this conclusion is based on the assumed relation between the local optical depth and geometrical thickness (given by the distribution 1 or 2 in this paper) which is not as simple for real clouds.

4.4. Discussion

Han and Ellingson (1999) and previous studies (Killen and Ellingson, 1994; Takara and Ellingson, 1996) addressed cloud scattering geometrical effects on their thermal radiative
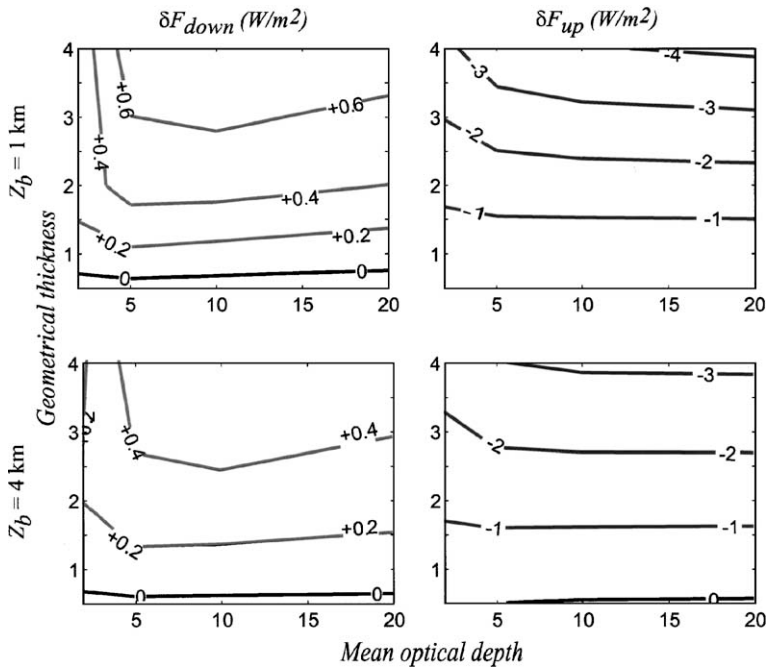
Fig. 15. Bias between fluxes of bumpy and flat clouds computed with 3D SHDOM in both cases as a function mean optical depth and mean geometrical thickness for two cloud base altitude ($Z_b = 1$, 4 km). Cloud Cl2 ($C = 58\%$) and distribution 2 ($\alpha = 0.7$) are considered.

properties in a GCM context. All these studies make use of the cloud "flat-plate" approximation. In the flat-plate approximation, a single-layer cloud field of cloud fraction C is simulated by a plane layer of infinitesimally thin but infinitively opaque ("black") clouds, with fractional coverage C. Therefore, this approximation neglects both cloud geometry and longwave optical properties. In order to take into account of these scattering or geometrical effects, they defined an effective cloud fraction C_{eff}, in such a way that this effective cloud fraction generates the same flux for a given broken cloud. In doing so, their problem is to determine the dependence of C_{eff} on different cloud parameters. These studies found effective cloud fraction function of cloud shape (cylinder, truncated conical clouds, etc.), aspect ratio, spatial distribution, scattering processes, thermal gradient between cloud top and its base and cloud coverage. Our work is quite different from these studies. In our paper, we analyze the difference between 3D fluxes simulated by SHDOM and three standard methods likely to be used in GCMs (PPH, CFPPH and IPA method). Since PPH, PPHCF and IPA fluxes are also computed with SHDOM model, and not from clouds in the flat/black plate approximation, our flux differences (3D-PPH, 3D-CFPPH, 3D-IPA) are also function of cloud geometric and optical properties (as earlier studies cited above). But our flux differences are not biased due to the "flat/black plate approximation" but about cloud structure. Moreover, and contrary to earlier studies, atmospheric gases are considered (primarily absorption by water vapor). Presence of

absorbing gas tends to reduce scattering effects (Takara and Ellingson, 1996). Therefore, quantitative comparison between our results and earlier results is not straightforward, even though some qualitative comparisons can be done (cloud inhomogeneity effects on their thermal radiative properties are sensitive functions of cloud coverage, of cloud base altitude and of cloud geometrical thickness).

5. Conclusions and outlook

In this paper, we presented a study of the effects of an inhomogeneous cloud layer with coverage on its large area-averaged thermal radiative fluxes. Fractional inhomogeneous clouds are generated for the first time by the "tdMAP" model. This new stochastic model shows great flexibility of use and is able to generate the complex self-similar structures of overcast and broken clouds. We show that tdMAP is suitable for simulating the 2D internal horizontal fluctuations of cloud optical properties observed in stratocumulus (quasi-lognormal distribution of optical depth, absolute spectral slope exponent around $\beta = 1.6$). The tdMAP model provides also an elegant method to simulate gaps between clouds by "pruning" the branches of the encoding tree with control by a Bernoulli parameter. Contrary to the bounded cascade process, tdMAP cloud structure does not have artificial dyadic structure and large increments between two consecutive cloud pixels. Moreover, edges of clouds are smooth (optical depth is generally small at the cloud periphery and larger within the cloud), which is not the case of the cubical or cylindrical cloud shapes used in previous studies.

Comparisons were done between fluxes of inhomogeneous clouds computed with 3D method (SHDOM model) and those computed by PPH, FCPPH and IPA methods. For better comparisons, fluxes computed by PPH, FCPPH and IPA methods are made also with SHDOM model using the appropriate settings to shut down horizontal transport. Biases thus estimated between 3D fluxes and PPH, FCPPH or IPA fluxes are only due to the drawback of the considered method.

Analysis of our results shows that thermal radiative fluxes depend primarily on cloud fraction, mean optical depth, mean geometrical depth and cloud base altitude. Horizontal fluctuation of the "within" cloud optical depth has a limited thermal radiative impact, for overcast cloud as well as broken cloud, and contrary to previous findings for solar wavelength (Cahalan et al., 1994a,b; Szczap et al., 2000a). The main cloud inhomogeneity parameters for thermal radiative transfer is the fractional cloud coverage parameter. Parameters relating to cloud distribution in space and cloud size distribution were not considered in this study, but should also be taken into account in the parameterization of the thermal radiative effects of inhomogeneous clouds (Takara and Ellingson, 1996; Han and Ellingson, 1999). Their effects on thermal radiative transfer for the more realistic and complex tdMAP clouds (compared to geometrical cuboids or cylinder clouds) have yet to be studied. This task will be the focus of a future study.

In this paper, we also compared inhomogeneous flat-top and bumpy-top clouds. Cloud top bumps are made by prescribing empirically justifiable relations gleaned from the literature between local optical depth and local geometrical thickness. We showed that effects of cloud bumps are rather small, especially when mean geometrical depth is smaller

than 1 km. This result is encouraging. Indeed, in a GCM, the atmosphere is divided into numerous layers, 20–100, depending on GCM vertical resolution. Therefore, clouds layers, in the troposphere, are rather thin. This means we can simplify a bumpy cloud layer by a flat top cloud layer with same mean geometrical depth as the GCM layer were they occur.

We demonstrated that the PPH method is not suitable to compute thermal inhomogeneous cloud fluxes, except for overcast clouds. FCPPH method and, more surprisingly the IPA method, are also not suitable to compute thermal inhomogeneous flat-top cloud fluxes, even though FCPPH and IPA biases are significantly smaller than their PPH counterparts. Both these methods lead to a bias of around ± 5 W/m^2 in upward or downward fluxes. This already non-negligible bias will be larger if the ground temperature is larger than the 288.1 K used in our work.

In future work, radiative transfer simulations will be done in solar wavelengths and across the whole thermal spectrum to investigate whether FCPPH and IPA biases remain on the complete (solar and thermal) spectrum. Also the fractal properties of tdMAP clouds will be examined. Finally, the case of multi-layer clouds will be investigated. Some preliminary results show that distance between cloud layers has to be considered in addition to the coefficient of correlation of the fractional cloud coverage between these cloud layers. All these sensitivity studies are necessary to determine the relevant cloud parameters in order to develop more accurate parameterizations of the effects of inhomogeneous cloud on radiative properties. Such efficient yet accurate radiative transfer parameterizations may be based, for example, on neural networks trained on many 3D simulations.

References

Aida, M., 1977. Scattering of solar radiation as a function of cloud dimensions and orientation. J. Quant. Spectrosc. Radiat. Transfer 14, 303–310.

Albrecht, B.A., Fairall, C.W., Thomson, D.W., White, A.B., Snider, J.B., 1990. Surface-base remote sensing of the observed and the adiabatic liquid water content of stratocumulus clouds. Geophys. Res. Lett. 17, 89–92.

Barker, H.W., 1994. Solar radiative transfer for wind-sheared cumulus cloud field. J. Atmos. Sci. 51, 1141–1156.

Barker, H.W., Wielicki, B.W., Parker, L., 1996. A parametrization for computing grid-average solar fluxes for inhomogeneous marine boundary layer cloud: Part II. Validation using satellite data. J. Atmos. Sci. 53, 2304–2316.

Barker, H.W., Morcrette, J.J., Alexander, G.D., 1998a. Broadband solar fluxes and heating rates for atmospheres with 3D broken clouds. Q. J. Meteorol. Soc. 124, 1245–1271.

Barker, H.W., Morcrette, J.J., Alexander, D.D., 1998b. Broadband solar fluxes and heating rates for atmospheres with 3D broken clouds. Q. J. Meteorol. Soc. 124, 1245–1271.

Barker, H.W., Stephens, G.L., Fu, Q., 1999. The sensitivity of domain-averaged solar fluxes to assumptions about cloud geometry. Q. J. Meteorol. Soc. 125, 2127–2152.

Benassi, A., 1995. Local self similar Gaussian process. In: Antoniadis, A., Oppenheim, G. (Eds.), Lecture Notes in Statistics, Wavelets and Statistics, vol. 103. Springer-Verlarg, New York, pp. 43–54.

Benassi, A., Deguy, S., 1999. Multi-scale fractional Brownian motion: definition and identification. Technical report, 83, LLIAC (Laboratoire de Logique, Algorithmique et Informatique de Clermont 1), Aubière, France.

Benassi, A., Jaffard, S., Roux, D., 1997. Gaussian processes and pseudo-differential elliptic operator. Rev. Mat. Iberoam. 13, 19–89.

Bréon, F.M., 1992. Reflectance of broken clouds fields: simulation and parameterization. J. Atmos. Sci. 49, 1221–1232.

Cahalan, R.F., 1989. Overview of fractal clouds. In: Deepak, A. (Ed.), Advances in Remote Sensing Retrieval Methods, 371–388. Hampton, Virginia.

Cahalan, R.F., Snider, J.B., 1989. Marine stratocumulus structure. Remote Sens. Environ. 28, 95–107.

Cahalan, R.F., Ridgway, W., Wiscombe, W.J., Bell, T.L., 1994a. The albedo of fractal stratocumulus clouds. J. Atmos. Sci. 51, 2434–2455.

Cahalan, R.F., Ridgway, W., Wiscombe, W.J., Bell, T.L., 1994b. Independent pixel and Monte Carlo estimates of stratocumulus albedo. J. Atmos. Sci. 51, pp. 3779–3790.

Cairns, B., Lacis, A.A., Carlson, B.E., 2000. Absorption within inhomogeneous clouds and its parameterization in general circulation models. J. Atmos. Sci. 57, 700–714.

Carvahlo, L.M., Silva Dias, M.A.F., 1998. An application of fractal box dimension to the recognition of mesoscale cloud patterns in infrared satellite images. J. Appl. Meteorol. 37, 1265–1282.

Chambers, L.H., Wielicki, B.A., Loeb, N.G., 2001. Shortwave flux from satellite-measured radiance. A theoretical study over marine boundary layer clouds. J. Appl. Meteorol. 40, 2144–2162.

Chandrasekar, S., 1960. Radiative Transfer. Dover, New York.

Chevallier, F., Chéruy, F., Scott, N.A., Chédin, A., 1998. A neural network approach for a fast and accurate computation of longwave radiative budget. J. Appl. Meteorol. 37, 1385–1397.

Davies, R., 1978. The effect of finite geometry on the three-dimensional of solar irradiance in clouds. J. Atmos. Sci. 35, 1712–1725.

Davis, J.M., Cox, S.K., McKee, T.B., 1978. Total shortwave radiative characteristics of absorbing finite clouds. J. Atmos. Sci. 36, 508–518.

Davis, A., Lovejoy, S., Schertzer, D., 1991. Discrete angle radiative transfer in multifractal medium. Proc.-SPIE 1558, 51–64.

Davis, A., Marshak, A., Cahalan, R., Wiscombe, W., 1994. Multifractal characterizations of non-stationarity and intermittency in geophysical fields, observed, retrieved or simulated. J. Geophys. Res. 54, 241–260.

Davis, A., Marshak, A., Wiscombe, W., Cahalan, R., 1996. Scale invariance of liquid water distribution in marine stratocumulus: Part I. Spectral properties and stationarity issues. J. Atmos. Sci. 53, 1538–1558.

Davis, A., Marshak, A., Cahalan, R., Wiscombe, W., 1997. The Landsat scale break in Stratocumulus as a three-dimensional radiative transfer effect: implication for cloud remote sensing. J. Atmos. Sci. 54, 241–259.

Davis, A., Marshak, A., Gerber, H., Wiscombe, W., 1999. Horizontal structure of marine boundary layer clouds from centimeter to kilometer scales. J. Geophys. Res. 104, 6123–6144.

Duroure, C., Guillemet, B., 1990. Analyse des hétérogénéités spatiales des stratocumulus et cumulus. Atmos. Res. 25, 331–350.

Ellingson, R.G., 1982. On the effects of cumulus dimensions on longwave irradiance and heating rates calculations. J. Atmos. Sci. 39, 886–896.

Evans, K.F., 1998. The spherical harmonics discrete ordinate method for three-dimensional atmospheric radiative transfer. J. Atmos. Sci. 55, 429–446.

Faure, T., Isaka, H., Guillemet, B., 2001a. Neural network analysis of the radiative interaction between neighboring pixels in inhomogeneous clouds. J. Geophys. Res. 106, 14465–14484.

Faure, T., Isaka, H., Guillemet, B., 2001b. Mapping neural network computation of high-resolution radiant fluxes of inhomogeneous clouds. J. Geophys. Res. 106, 961–974.

Frisch, U., 1995. Turbulence—The Legacy of A.N. Kolmogorov. Cambridge University Press, Cambridge, UK.

Fu, Q., Liou, K.N., 1992. On the correlated k-distribution method for radiative transfer in nonhomogeneous atmospheres. J. Atmos. Sci. 49, 2139–2156.

Fu, Q., Cribb, M., Barker, H., Krueger, S.K., Grossman, A., 2000. Cloud geometry effects on atmospheric solar absorption. J. Atmos. Sci. 57, 1156–1168.

Gotoh, K., Fujii, Y., 1998. Fractal dimension analysis on the cloud shape parameter of cumulus over land. J. Appl. Meteorol. 37, 1283–1292.

Gube, M., Schmetz, J., Raschke, E., 1980. Solar radiative transfer in cloud field. Contrib. Atmos. Phys. 53, 24–34.

Han, D., Ellingson, R.G., 1999. Cumulus cloud formations for longwave radiation calculations. J. Atmos. Sci. 56, 837–851.

Harshvardhan, Weinman, J.A., 1982. Infrared radiative transfer through a regular array of cuboidal clouds. J. Atmos. Sci. 39, 431–439.

Jeffery, C.A., 2001. Investigating the small-scale structure of clouds using the delta-correlated closure. Atmos. Res. 59–60, 199–215.

Jonas, P.R., 1994. On the reflectance of cellular cloud layers. Q. J. Meteorol. Soc. 120, 221–229.

Kassianov, E.I., Kogan, Y.L., 2002. Spectral dependence of radiative horizontal transport in stratocumulus clouds and its effect on near-IR absorption. J. Geophys. Res. 107, AAC15-1–AAC15-13.

Killen, R.M., Ellingson, R.G., 1994. The effect of shape and spatial distribution of cumulus on longwave irradiance. J. Atmos. Sci. 51, 2123–2136.

Kobayashi, T., 1993. Effects due to cloud geometry on biases in the albedo derived from radiance measurements. J. Clim. 6, 120–128.

Kolmogorov, A.N., 1962. A refinement of previous hypothesis concerning the local structure of turbulence in viscous incompressible fluid at high Reynolds number. J. Fluid Mech. 13, 82–85.

Krasnopolsky, V.M., Chevallier, F., 2003. Some neural network application in environment sciences: Part II. Advancing computation efficiency of environmental numerical models. Neural Netw. 16, 335–348.

Lenoble, J., 1985. Radiative Transfer in Scattering and Absorbing Atmosphere: Standard and Computational Procedures A. Deepak Publication, Hampton.

Lovejoy, S., 1982. Area-parameter relation for rain arid cloud areas. Science 216, 185–237.

Lovejoy, S., Mandelbrot, B.B., 1985. Fractal properties of rain, and a fractal model. Tellus 37, 209–232.

Maedor, W.E., Waever, W.R., 1980. Two-stream approximation to radiative transfer in planetary atmospheres: a unified description of existing model and new improvement. J. Atmos. Sci. 37, 630–643.

Mandelbrot, B.B., Van Ness, J., 1968. Fractional Brownian motion, fractional noises and applications. SIAM Rev. 10, 422–437.

Marshak, A., Davis, A., Wiscombe, W., Cahalan, R., 1995a. Radiative smoothing in fractal clouds. J. Geophys. Res. 100, 26247–26261.

Marshak, A., Davis, A., Wiscombe, W., Titov, G., 1995b. The verisimilitude of the independent pixel approximation used in cloud remote sensing. Remote Sens. Environ. 52, 71–78.

Marshak, A., Davis, A., Wiscombe, W., Cahalan, R., 1997. Scale invariance in liquid water distribution in marine stratocumulus: Part II. Multifractal properties and intermittency issues. J. Atmos. Sci. 54, 1432–1444.

McKee, T.B., Cox, S.K., 1974. Scattering of visible radiation by finite clouds. J. Atmos. Sci. 31, 1885–1892.

Minnis, P., Heck, P.W., Young, D.F., Fairall, C.W., Snider, J.B., 1992. Stratocumulus cloud properties derived from simultaneous satellite and island-based instrument during FIRE. J. Appl. Meteorol. 31, 317–339.

Nakajima, T.Y., Nakajima, T., 1995. Wide-area determination of cloud microphysical properties from NOAA AVHRR measurements for FIRE and ASTEX regions. J. Atmos. Sci. 52, 4043–4059.

Nasunaga, H., Nakajima, T., 2001. The effective cloud fraction of broken clouds obtained by multistream radiative transfer: Part I. Longwave radiation. J. Atmos. Sci. 58, 2455–2467.

Novikov, E.A., Stewart, R., 1964. Intermittency of turbulence and spectrum of fluctuations in energy dissipation. Izv. Akad. Nauk SSSR, Ser. Geofiz. 3, 408–412.

O'Hirok, W., Gauthier, C., 1998. A three-dimensional radiative transfer model to investigate the solar radiation within a cloudy atmosphere: Part I. Spatial effects. J. Atmos. Sci. 55, 2162–2179.

Schertzer, D., Lovejoy, S., 1991. Nonlinear geodynamical variability: multiple singularities, universality and observables. In: Schertzer, D., Lovejoy, S. (Eds.), Scaling, Fractals and Non-linear Variability in Geophysics. Kluwer Academic, Dordrecht-Boston, pp. 41–82.

Schmetz, J., 1984. On the parameterization of the radiative properties of broken clouds. Tellus 36, 417–432.

Szczap, F., Isaka, H., Saute, M., Guillemet, B., 2000a. Effective radiative properties of bounded cascade non-absorbing clouds: definition of the equivalent homogeneous cloud approximation. J. Geophys. Res. 105, 20617–20634.

Szczap, F., Isaka, H., Saute, M., Guillemet, B., 2000b. Effective radiative properties of bounded cascade absorbing clouds: definition of effective single scattering albedo. J. Geophys. Res. 105, 20635–20648.

Szczap, F., Isaka, H., Saute, M., Guillemet, B., Gour, Y., 2000c. Inhomogeneity effects of 1D and 2D bounded cascade model clouds on their effective radiative properties. Phys. Chem. Earth 25, 83–89.

Takara, E.E., Ellingson, R.G., 1996. Scattering effects on longwave fluxes in broken cloud fields. J. Atmos. Sci. 53, 1464–1476.

Titov, G.A., 1998. Radiative horizontal transport and absorption in stratocumulus clouds. J. Atmos. Sci. 55, 2549–2560.

Zuev, V.E., Titov, G.A., 1995. Radiative transfer in cloud field with random geometry. J. Atmos. Sci. 52, 176–177.